Discover Applied Sciences

Research

Bioinspired synthesis and characterization of zinc oxide nanoparticles and assessment of their cytotoxicity and antimicrobial efficacy

Rajeev Acharya¹ · Felix Tettey^{2,3} · Aakash Gupta⁴ · Khaga Raj Sharma¹ · Niranjan Parajuli¹ · Narayan Bhattarai²

Received: 7 November 2023 / Accepted: 6 February 2024

Published online: 21 February 2024 © The Author(s) 2024 OPEN

Abstract

Zinc oxide nanoparticles (ZnO NPs) are versatile and promising, with diverse applications in environmental remediation, nanomedicine, cancer treatment, and drug delivery. In this study, ZnO NPs were synthesized utilizing extracts derived from *Acacia catechu, Artemisia vulgaris*, and *Cynodon dactylon*. The synthesized ZnO NPs showed an Ultraviolet–visible spectrum at 370 nm, and X-ray diffraction analysis indicated the hexagonal wurtzite framework with the average crystallite size of 15.07 nm, 16.98 nm, and 18.97 nm for nanoparticles synthesized utilizing *A. catechu, A. vulgaris*, and *C. dactylon* respectively. Scanning electron microscopy (SEM) demonstrated spherical surface morphology with average diameters of 18.5 nm, 17.82 nm, and 17.83 nm for ZnO NPs prepared from *A. catechu, A. vulgaris*, and *C. dactylon*, respectively. Furthermore, ZnO NPs tested against *Staphylococcus aureus, Kocuria rhizophila, Klebsiella pneumonia*, and *Shigella sonnei* demonstrated a zone of inhibition of 8 to 14 mm. The cell viability and cytotoxicity effects of ZnO NPs were studied on NIH-3T3 mouse fibroblast cells treated with different concentrations (5 μg/mL, 10 μg/mL, and 50 μg/mL). The results showed biocompatibility of all samples, except with higher doses causing cell death. In conclusion, the ZnO NPs synthesized through plant-mediated technique showed promise for potential utilization in various biomedical applications in the future.

Highlights

- Bioinspired synthesis of ZnO NPs utilizing plant extracts of Acacia catechu, Artemisia vulgaris, and Cynodon dactylon.
- Characterization of ZnO NPs through Ultraviolet-visible Spectroscopy, Fourier-transform Infrared Spectroscopy, X-ray Diffraction, Scanning Electron Microscopy, and Energy-dispersive X-ray Spectroscopy.
- Evaluation of antibacterial effects of ZnO NPs.
- Cytotoxicity and cell viability assays of nanoparticles.

Rajeev Acharya and Felix Tettey contributed equally to the study.

Supplementary Information The online version contains supplementary material available at https://doi.org/10.1007/s42452-024-05719-2.

Miranjan Parajuli, niranjan.parajuli@cdc.tu.edu.np; Marayan Bhattarai, nbhattar@ncat.edu; Rajeev Acharya, acharyarajeev19@ gmail.com; Felix Tettey, fatettey@aggies.ncat.edu; Aakash Gupta, gupta_aakash_007@yahoo.com; Khaga Raj Sharma, Khaga.sharma@cdc.tu.edu.np | ¹Central Department of Chemistry, Tribhuvan University, Kirtipur 44618, Nepal. ²Department of Chemical, Biological, and Bioengineering, North Carolina A&T State University, Greensboro, NC 27411, USA. ³Department of Industrial and Systems Engineering, North Carolina A&T State University, Greensboro, NC 27411, USA. ⁴Department of Chemistry and Biochemistry, University of Massachusetts Dartmouth, North Dartmouth, MA 02747, USA.



Discover Applied Sciences

(2024) 6:85

| https://doi.org/10.1007/s42452-024-05719-2



Keywords Zinc oxide nanoparticles · Natural Products · Secondary Metabolites · Cytotoxicity

1 Introduction

Nanotechnology is one of the most active areas of research in modern material science which provides the capability to manipulate the material properties through precise control of their size and morphology. It is gaining prominence across various sectors such as healthcare, beauty products, computers, optics, catalysis, food technology, biomedical applications, pharmaceutical companies, and environmental remediation [1, 2]. The tiny size and the remarkable surface-to-volume ratio of nano-sized materials make them so interesting that they exhibit greater reactivity compared to bulk materials [3]. Among a variety of metal oxide nanoparticles like TiO₂, FeO, CuO, SiO₂, and NiO, ZnO is highly favored due to simplicity in synthesis, remarkable selectivity, biocompatibility, non-toxicity, enhanced optoelectronic properties [4], and significant band gap of approximately 3.37 eV, and an elevated exciton binding energy of 60 meV [5].

As per the safety data sheet provided by USFDA, ZnO falls under the categorization of a "Generally Recognized as Safe" (GRAS) material and demonstrates antibacterial, antifungal, antidiabetic, and anticancer properties [6]. These properties are ascribed to their tiny dimensions that possess the capacity to enter and move through, allowing them to breach the biological barriers, disrupt cellular functions, and navigate through various biological systems of the host resulting in uncontrolled cell proliferation and death [7]. The antimicrobial effect of ZnO NPs arises from either direct adherence to cell walls or indirectly generating reactive oxygen species (ROS) upon exposure to biological fluids or moisture that causes oxidative stress, disrupting microbial membranes, functions, enzymatic activity, and replication ultimately inhibiting microorganisms [8, 9]. The ROS mentioned above under physiological conditions, induces cellular damage and triggers apoptosis [10], and is responsible for anticancer activities. Additionally, ZnO NPs disrupt mitochondrial function [11] and interfere with cell division and proliferation in cancerous cells. These properties supported by biocompatibility, non-toxicity, ease of fabrication, and remarkable selectivity [12, 13], of ZnO NPs, collectively make them promising candidates for further exploration in anticancer studies [13, 14]. ZnO NPs have been produced through traditional physical and chemical approaches such as laser ablation [15], ball milling [16], sputtering [17], sol-gel technique [18], chemical vapor deposition [19], microemulsion [20], and hydrothermal methods [21]. A more energy-efficient, beneficial, lesser complications, economical, and eco-friendly green approach has emerged, that entails the utilization of plant extracts, microorganisms, and biowaste materials and facilitates large-scale production at room temperature and overcomes the drawbacks of conventional techniques like the need for energetic processes, huge quantities of chemical substances, low output, cost and toxicity [22-24]. Plant-mediated NP synthesis is carried out in three phases; reduction phase where metal ions from salt precursors undergo a reduction process from a higher oxidation state (O.S) to zero O.S which facilitates the nucleation of metal atoms, growth phase where the reduced metal aggregates and nucleates gradually to form NPs and stabilization phase where synthesized NPs are stabilized through a capping mechanism of plant metabolites [25–28]. Plant-based biomolecules like polyphenols, polysaccharides, alkaloids, vitamins, and flavonoids, function as both reducing and capping agents in NPs formation [29–31]. The concentration of metal salt [32], type of plant extracts [33], solution pH [33], reaction time, and annealing temperature [32], significantly influence the shape, size, and overall quality of NPs synthesized through plant-mediated methods. Synthesis of ZnO NPs using orange peel extract [34], Artemisia pallens [35], Scoparia dulcis [22], Hibiscus sabdariffa [36], Bixa Orellana [14], Xanthomonas oryzae [37], Hagenia abyssinica [4], Pandanus odorifer [38], Cassia fistula [39], grape seed [40], Euphorbia abyssinica [41], and Cocos nucifera [42], had been previously studied for antimicrobial activities.

Similarly, in this work leaves of *Acacia catechu*, *Artemisia vulgaris*, and *Cynodon dactylon* were utilized for synthesizing ZnO NPs. *A. catechu* is a deciduous tree that is a member of the Fabaceae family and is native to South Asia, specifically in India, Nepal, and Myanmar. It is utilized for treating a variety of health issues and contains phytochemicals such as carbohydrates, proteins, thiols, tannins, phenolics, alkaloids, flavonoids, and glycosides [43]. *A. vulgaris* is a perennial herb belonging to the Asteraceae family and is naturally occurring in Europe, Asia, and North Africa. It has been utilized in the management of digestive disorders, menstrual issues and as a tonic and contains phytochemicals, including flavonoids, essential oils, amino acids, carbohydrates, polyphenols, saponins, and tannins [44]. *C. dactylon* is an evergreen turf that flourishes in warm climates of the Poaceae family, originating from Africa, Asia, and Australia. It has been traditionally employed in herbal medicine due to its therapeutic advantages [45]. The phytochemicals of *C. dactylon* include flavonoids, alkaloids, steroids, terpenoids, triterpenoids, saponins, resins, tannins, fixed oils, and reducing sugars [46]. The purpose of this study was to synthesize ZnO NPs utilizing locally available plants with therapeutic values namely *A. catechu*, *A. vulgaris*, and *C. dactylon* leaf extracts, and characterize the synthesized ZnO NPs through Ultraviolet–visible (UV–Vis),



Fourier-transform infrared spectroscopy (FTIR), X-ray diffraction (XRD), Scanning electron microscopy (SEM), and Energy Dispersive X-ray spectroscopy (EDX). Furthermore, the study seeks to investigate the antibacterial and cytotoxicity properties of the synthesized ZnO NPs. In summary, this research centers on a bioinspired method for synthesizing ZnO NPs, utilizing plant extracts. Unlike conventional techniques that involve the use of harsh chemicals and energy-intensive processes, our approach ensures a contribution to a sustainable and eco-friendly NPs synthesis route. One key advantage of this bioinspired synthesis lies in the improved biocompatibility of the resulting ZnO NPs. By utilizing the unique properties associated with plant metabolites, our method imparts biocompatible characteristics to the nanoparticles, rendering them more appropriate for biomedical applications, without compromising efficacy.

2 Materials and methods

2.1 Materials

Leaves of *A. catechu* and *A. vulgaris*, as well as the leaves and roots of *C. dactylon*, were collected from the wild of Simara city (27.1600° N, 84.9700° E), Bara district of Nepal, and their identification was confirmed by the Tribhuvan University Central Herbarium, Nepal. Every chemical employed in this study was of analytical grade. Zn (NO)₃.6H₂O, NaOH, and ethanol were procured from Sigma-Aldrich, MA, USA. Moreover, nutrient agar (NA), Mueller Hinton Agar (MHA), and Mueller Hinton Broth (MHB) were procured from HiMedia (India). Dulbecco's modified Eagle's medium (DMEM) and Dulbecco's phosphate-buffered saline (DPBS) were sourced from Life Technologies (Grand Island, NY, USA). Alamar Blue and lactate dehydrogenase (LDH) assay kits were purchased from Thermo Fisher Scientific, MA, USA.

2.2 Preparation of plant extracts

After collection, the plant parts were extensively rinsed with water and shade-dried for 2 weeks. The plant parts were ground finely with the help of an electric blender and then kept in air-tight plastic bags for further utilization [1]. 1 g of fine powder of plants (*A. catechu, A. vulgaris, C. dactylon*) was blended with 50 mL of distilled water in a beaker. The mixture was stirred at 60 °C followed by a water bath treatment at the same temperature for 1 h. The resultant suspension underwent filtration through Whatman No. 1 filter paper and was subsequently stored at 4 °C for further use [34].

2.3 Synthesis of ZnO NPs

2 g of $Zn(NO)_3$.6 H_2O was weighed and combined with 42.5 mL of respective plant extract in a beaker to prepare a 0.15 M suspension, followed by stirring for 1 h following the protocol suggested by Thi et al. [34]. The mixture pH was maintained to 9 which is basic. Subsequently, the mixture was introduced into a water bath at 60 °C for 1 h and subjected to hot air drying in an oven at 150 °C, and the resulting residue was washed with ethanol 2–3 times followed by drying overnight in a desiccator. Finally, it was placed in the muffled furnace, maintained at 400 °C for about 2 h, and powdered nanoparticles were obtained which were then stored in Eppendorf tubes for further characterization [34]

2.4 Characterization of ZnO NPs

The ZnO NPs synthesized utilizing plant-mediated methods were subjected to morphological characterization through several techniques such as UV–visible spectroscopy, Fourier-transform infrared spectroscopy (FTIR), X-ray diffraction (XRD), Scanning electron microscopy (SEM), and EDX. The confirmation of ZnO NPs synthesis was accomplished by analyzing the absorption band detected using a UV–visible spectrophotometer (SPECORD 200 PLUS, Analytik Jena, Germany) within 300–650 nm. Similarly, the stretching of the Zn–O bond and secondary metabolites present in the plant extracts was investigated through FTIR (IR Tracer 100-Shimadzu, Japan), analyzed in the spectral range within (4000–400) cm⁻¹. To determine the degree of crystallinity in the synthesized ZnO NPs, an X-ray diffraction pattern was acquired utilizing the (Rigaku D/MAX-2500/pc diffractometer, Germany) with monochromatic Cu Kα radiation of wavelength 1.5406 Å, 20 scanned within the interval of 20–80°. The size of the ZnO NPs crystallites was determined with Scherrer's equation [47], as follows:



$$D = \frac{k\alpha}{\beta \cos \theta} \tag{1}$$

Where D = Crystallite or grain size; K = dimensionless shape factor, with a value approximately close to unity (\approx 0.9); λ =Wavelength of X-ray radiation employed, (0.15406 nm for CuK α); θ = Bragg's angle (half of 2 θ value of the selected peak; in radians); β = Full-width half maximum (FWHM, in radians).

The surface composition and particle size of ZnO NPs were analyzed through SEM (JSM-7600/JEOL, Korea) coupled with EDX (JEM-2100F/JEOL, Korea) to find out the elemental composition of NPs functioned at a voltage of 10 kV.

2.5 Antibacterial activity of ZnO NPs

The antibacterial effects of ZnO NPs derived from *A. catechu, C. dactylon,* and *A. vulgaris* were assessed through the disc diffusion method [48]. The sterile cotton swab was used to spread a freshly prepared microbial culture of test organisms (*Staphylococcus aureus* (SA), *Klebsiella pneumoniae* (KP), *Shigella sonnei* (SS), and *Kocuria rhizophila* (KR)) onto an MHA plate. ZnO NPs (50 mg/mL), neomycin (1 mg/ mL, positive control), water (negative control), plant extract (20 mg/mL), blank A (20 mg/mL), and blank B (50 mg/mL) suspension/solution were loaded separately into sterile antimicrobial susceptibility discs and then put upon an MHA plate and incubated at 37 °C for 18–24 h. Following the designated incubation period, the zone of inhibition (ZOI) was assessed along with the antimicrobial disc and noted in mm.

2.6 Dose-response toxicity study of plant-mediated synthesized ZnO particles

All the ZnO NPs powder before exposure with the cells was UV-sterilized, suspended in ethanol for 15 min utilizing ultrasonication (Branson Ultrasonic Corporation, Danbury, CT, USA), and centrifuged (Z206-A Compact Centrifuge, Benchmark Scientific Inc, NJ, USA) at 4500 rpm for 10 min. The particles were then autoclaved and dispersed in a cell culture medium, DMEM supplemented with 10% serum. 1 mL of the particle suspension was treated with the cells. Before treatment with the cells, the NIH-3T3 cells, a mouse fibroblast cell line (ATTC 1658, Manassas, VA, USA) with a start density of 5×10^4 was cultured in DMEM in a 48-well plate. After cells attained about 70% confluence, they were treated with different concentrations (i.e. $5 \mu g/mL$, $10 \mu g/mL$, and $50 \mu g/mL$ of the ZnO NPs in a cell culture medium) and preserved in a humidified environment enriched with 5% CO $_2$ at 37 °C for 72 h [49–51]. The ZnO NPs samples from *A. catechu* were represented as AC-5, AC-10, and AC-50 whereas those from *A. vulgaris* were labeled as AV-5, AV-10, and AV-50. Additionally, those from *C. dactylon* were identified as CD-5, CD-10, and CD-50. Cells without treatment with the ZnO NPs were considered the control and labeled AC-0, AV-0, and CD-0. $100 \mu L$ was obtained from the culture medium for all assays and all treatments were repeated three times.

2.7 Cytotoxicity assay

The fibroblast cell-particle medium's supernatant was collected at predetermined time intervals (24 h, 48 h, and 72 h) and preserved for subsequent cytotoxicity analysis. The impact of the ZnO NPs on the fibroblast cells' cytotoxicity was determined through the Pierce lactate dehydrogenase (LDH) cytotoxicity assay kit, following the methods outlined in our prior publication [52, 53]. In brief, 50 μ L of each preserved supernatant was triplicated in a fresh 96-well flat-bottom plate. To each sample in the well plate, 50 μ L of the reaction mixture as directed by the manufacturer's instructions was added, and the 96-well plate was placed in darkness for 30 min. The positive and negative controls were established as per the manufacturer's instructions. The reaction was halted by adding 50 μ L of the stop solution with gentle tapping. The absorbance of the test solution in the well plate was evaluated at 490 nm and 680 nm absorbance using a CLARI-Ostar® multi-mode plate reader (BMG LABTECH Inc., Cary, NC, USA). The cytotoxicity was assessed utilizing the provided equation:

$$Cytotoxicity = \frac{OD \text{ at } 490 \text{ nm test sample} - OD \text{ at } 490 \text{ nm negative control}}{OD \text{ at } 490 \text{ nm positive} - OD \text{ at } 490 \text{ nm negative control}} \times 100\%$$
(2)

where OD is the absorbance.



2.8 Cell viability assay

The Alamar Blue (AB) colorimetric test was utilized to assess the vivacity of the 3T3 cells utilizing protocol from the manufacturer and our previous publications [54, 55]. For this test, excess media in the experimental well plate was taken out and the well plate was rinsed twice with PBS. A 5% (v/v) solution of AB reagent in the appropriate culture medium (50 μ L of AB reagent dissolved in 1 mL of culture medium) was added to the well plate and incubated for 4 h. The test solutions were moved to new well plates, and fluorescence was subsequently measured with a microplate reader (CLARIOstar Plus, BMG LABTECH Inc., Cary, NC, USA) with excitation at 530 nm and emission at 590 nm. The cell viability was determined with the following equation:

$$CellViability = \frac{Fluorescence of the sample - Fluorescence of the blank}{Fluorescence of the control - Fluorescence of the blank} \times 100\%$$
(3)

The viable cell morphology was observed using a fluorescence microscope on day 3. Before imaging, the cells underwent two PBS washes, were fixed with a 4% paraformaldehyde (PFA, Thermofisher Scientific) solution for 10 min, and then permeabilized with 0.2% triton (X-100) (Thermofisher Scientific) for 2 min at room temperature. The cells underwent PBS washing and were then blocked using 1% bovine serum albumin (BSA) for 30 min. The cells were subsequently stained with rhodamine-phalloidin (red) for cytoskeleton (Invitrogen, Thermo Fisher Scientific) for 20 min and DAPI (4'6, -diamidino-2-phenylindole, dihydrochloride; Invitrogen, Thermofisher Scientific), for nuclei also for 5 min both under dark conditions at room temperature. Following three rounds of PBS washing, fluorescence images were captured with an Olympus I × 83 microscope (Olympus).

2.9 Statistical analysis

All in vitro experiments were independently conducted in triplicate, and the data acquired underwent statistical analysis utilizing one-way analysis of variance (ANOVA) along with Tukey's post hoc test. The statistical significance of all data was determined utilizing OriginPro 2023 Version software (Origin Lab, Northampton, MA, USA) and expressed as the mean \pm standard deviation, at n = 3) with statistical significance denoted by *p < 0.05 and **p < 0.01.

3 Results and discussion

3.1 Synthesis of ZnO NPs

The formation of ZnO NPs is commonly indicated by a noticeable alteration in the solution's color. The introduction of zinc precursors to the plant extracts triggers the reduction of zinc ions, leading to the formation of ZnO. This reduction is accompanied by an observable shift in the color of the reaction mixture, transitioning from dark brown to light brown which ensured the synthesis of ZnO NPs. This color change is best matched in previous literature [56]. Further, the white powdered form is obtained after treatment with a muffled furnace at 400 °C for about 2 h. The phytochemicals play a major role as both reducing and capping agents in the eco-friendly synthesis of ZnO NPs. The metabolites in A. catechu extracts include tannins, terpenoids, triterpenoids, alkaloids, ascorbic acid, carbohydrates, resins, saponins, and flavonoids [20, 57]. In a study led by Adhikari et.al., Gas chromatography-mass spectrometry (GC-MS) analysis revealed that A. catechu leaf extract constituents, including, catechin, epicatechin, acacatechin, 4-hydroxybenzoic acid, mesquitol, kaempferol, baicalin, and quercetin [58–60]. Similarly, the phytochemical analysis of A. vulgaris extract showed the occurrence of flavonoids, coumarins, volatile oils, sesquiterpenes, lactones, inulin, and a small number of alkaloids that have been characterized by (GC-MS) [61, 62]. Likewise, fatty acids (palmitic acid, stearic acid, oleic acid, and linoleic acid), tocopherol content, sterol compounds, and phenolic compounds (hydroguinone, glycerine, thymol, phytol, and ethyl glucopyranoside) were known from C. dactylon extract [63]. In the process of bioinspired ZnO NPs synthesis, zinc ions (Zn^{2+}) derived from the precursor are found in the reaction medium. The reduction of Zn^{2+} to Zn^0 is frequently facilitated by the phytochemicals in plant extracts including phenols, flavonoids, and terpenoids which donate electrons in a redox reaction to the zinc ions, initiating the nucleation and subsequent growth of ZnO NPs. Additionally, These phytochemicals not only serve as substances that reduce but also contribute to NPs stabilization by binding to their surface, preventing



agglomeration, and ensuring colloidal solution stability [27]. The method employed to synthesize ZnO NPs has benefits like eco-friendliness, biocompatibility, affordable, and efficiency while using natural resources. However, the practicality of large-scale synthesis using green sources from an industrial and commercialization perspective involves the consideration of factors like scalability; in which the variability of natural sources and specific conditions needed for green synthesis may pose challenges in maintaining consistency, reproducibility, and product quality on a larger scale [64–66].

3.2 UV Spectroscopy analyses

The presence of absorption maxima at 372 nm (*A. catechu*), 370 nm (*A. vulgaris*), and 368 nm (*C. dactylon*) as depicted in Fig. 1 verified the existence of ZnO NPs prepared from three different plant extracts which are similar to various literature [2, 35, 67]. The absorption maxima observed at approximately 370 nm is ascribed to ZnO's inherent absorption band gaps, arising from the excitation of electrons moving from the valence band to the conduction band (O $2p \rightarrow Zn$ 3d) [68].

Blank A is prepared without adding Zinc nitrate hexahydrate while Blank B is prepared by excluding the plant extract by synthesis protocol.

The intrinsic band gap energy (Eg) for ZnO NPs derived from A. catechu, A. vulgaris, and C. dactylon were observed to be 3.40 eV, 3.42 eV, and 3.35 eV respectively, as depicted in Figure S3, S2, and S1 utilizing the Tauc plot equation;

$$\left[\alpha h v = C \left(h v - E g\right)\right]^{m} \tag{4}$$

Where α = absorbance coefficient, C = constant, h = Planck's constant, v = photon frequency, Eg = optical band gap, and m = 1/2 for direct band gap semiconductors.

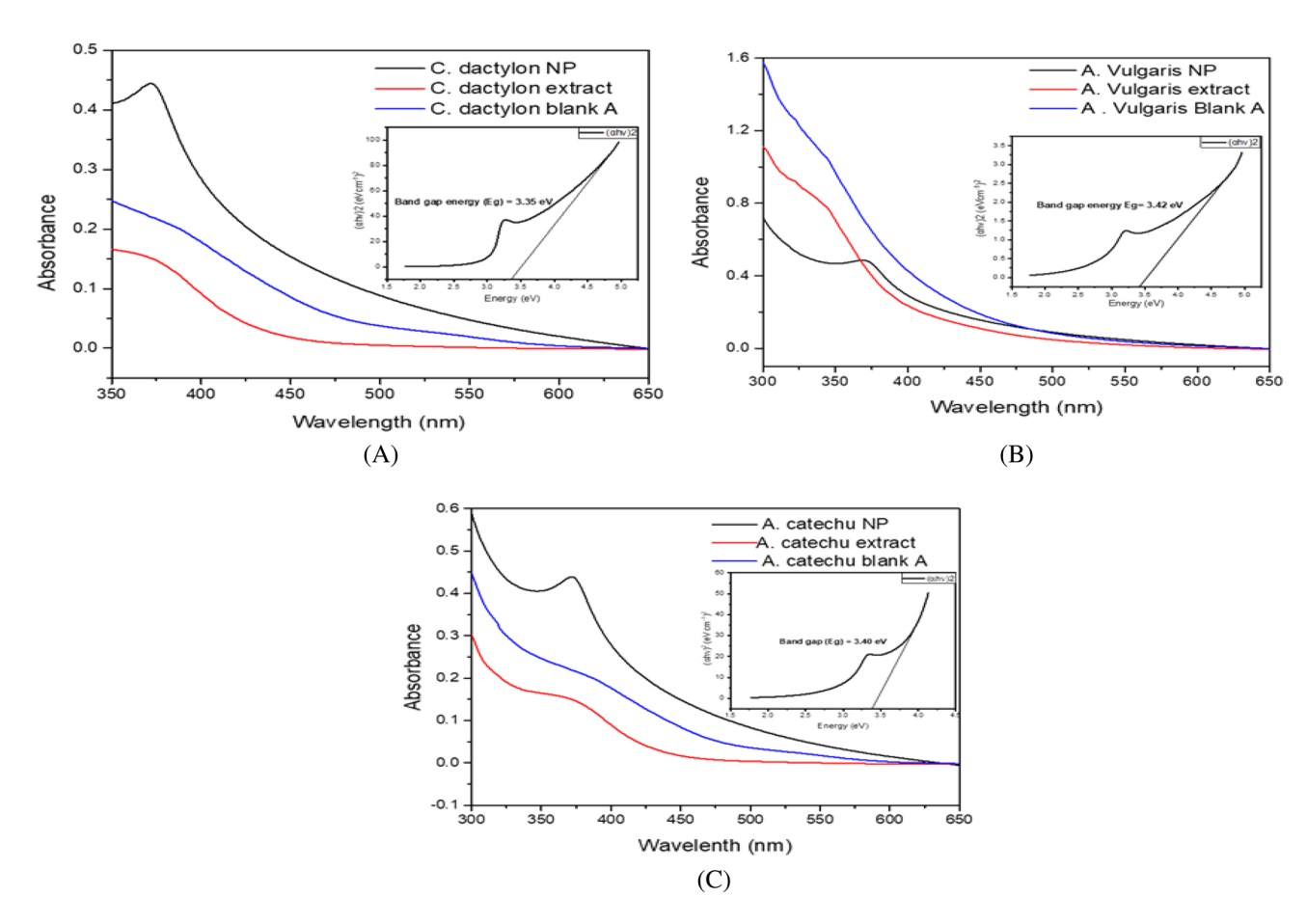


Fig. 1 UV–Vis Spectroscopy of Plant extracts, blank test, ZnO NPs synthesized from **A** *C. dactylon,* **B** *A. vulgaris,* and **C** *A. catechu* respectively along with tauc plots in the inset



The values obtained were close to the theoretical value of 3.37 eV. The band gap values were derived through the extension of the linear section of $(\alpha hv)^2$ against the hv plot until it intersected with the X-axis [35]. The elevated band gap energy suggested ZnO NPs obtained through plant extract require higher energy to stimulate electrons from the valence to the conduction band [69]. The observed results are consistent with several literature reports, where the absorption maximum of ZnO NPs within (340–378) nm, corresponds to a band gap energy extending from 3.1 to 3.4 eV [2, 14, 68].

3.3 FTIR spectroscopy analyses

The FTIR analysis revealed the existence of diverse functional groups originating from plant extracts, which act as both reducing and capping agents. The detected peaks within the (400–600) cm⁻¹ range as shown in Fig. 2 are typically linked with the interaction between metal and oxygen [35]. In particular, the existence of a peak at around 420 cm⁻¹ indicates the stretching vibration of the Zn–O bond, confirming the existence of ZnO NPs. The peaks noted at approximately 840 and 880 cm⁻¹ are indicative of the generation of zinc tetrahedral coordination [71]. The appearance of a peak at 1066 cm⁻¹ is a result of the stretching vibration of the C–O–C bond. The peaks around 1436 cm⁻¹ imply bending bands related to C–O–H, whereas the peak around 1752 cm⁻¹ indicates C=O stretching vibration signifying aldehyde and ketone functionality. A peak near 2340 cm⁻¹ is associated with the nitrile group, indicating the presence of a nitrogen-containing group from plant extract. Finally, the peak close to 2980 cm⁻¹ is a result of the stretching vibration of C-H bonds mostly of the aromatic system. All of these peaks align with those found in the literature for ZnO NPs that were synthesized using green methods [2, 35, 71]. Thus, the FTIR spectrum revealed plant-synthesized ZnO NPs along with different functionalities arising due to phytochemicals found in the plant extract.

Similarly, The FTIR spectrum of *C. dactylon* extract exhibited prominent peaks at various wavenumbers; 3273 cm⁻¹ (resulting from O–H bond stretching), 2980 cm⁻¹ (C–H stretching), 2338 cm⁻¹ (N–H stretching), 1592 cm⁻¹ (associated with C=C bond vibration), and 1394 cm⁻¹ along with 1341 cm⁻¹ (related to C-H bending) [72, 73]. Likewise, The FTIR spectrum of *A. vulgaris* extract exhibited prominent peaks at various wavenumbers: 3424 cm⁻¹ (broad peak revealing the presence of a strong H-bonded hydroxyl group associated with alcohol, phenols, or carboxylic acid), 2971 cm⁻¹ and 2900 cm⁻¹ (resulting from C-H bond stretching), 2334 cm⁻¹ (related with stretching mode of the CO group) and 1648 cm⁻¹ (associated with the CO group in amides) [74]. Finally, looking at the FTIR spectrum of *A. catechu* extract, peaks around 3273 cm⁻¹ (corresponds to -OH stretching), 2980 and 2900 cm⁻¹ (suggests the presence of C-H bonds), 2301 cm⁻¹ (associated with -CN group), 1564 and 1398 cm⁻¹ (suggests the carbonyl groups in ketone and esters) [75]. Thus, the result indicates the existence of flavonoids, phenols, amines, amino acids, etc. in plant extracts that play a role in reducing and capping ZnO NPs during the synthesis process.

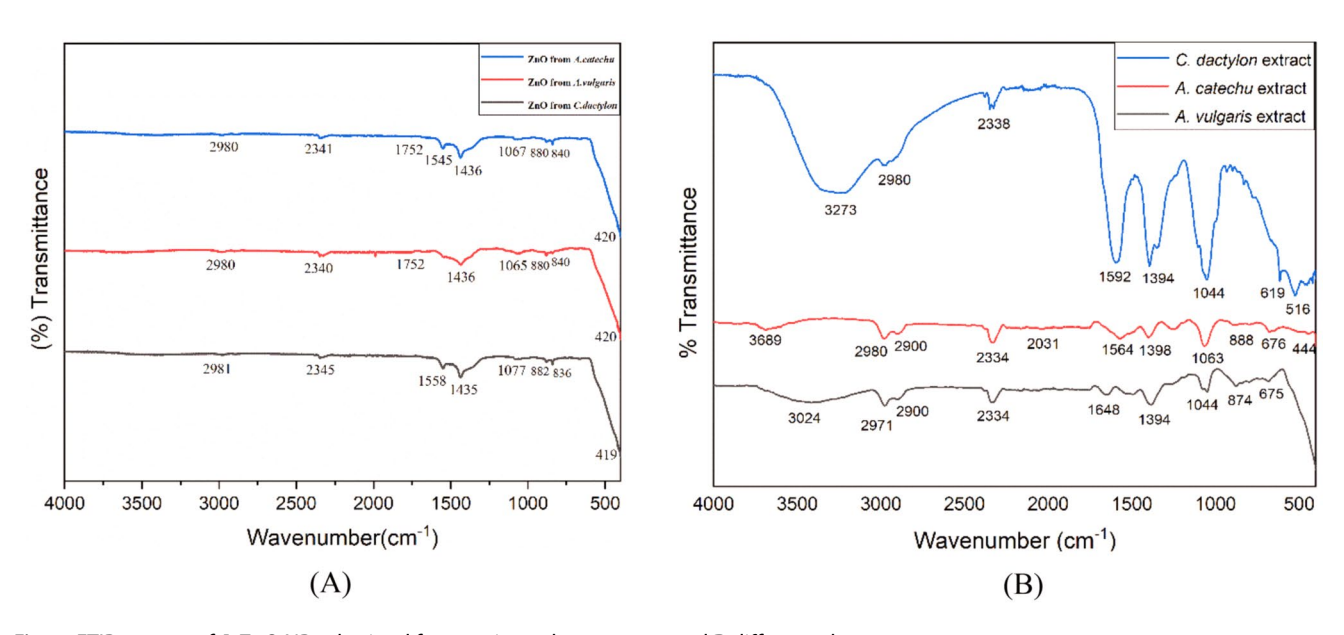


Fig. 2 FTIR spectra of **A** ZnO NPs obtained from various plant extracts and **B** different plant extract



3.4 X-ray diffraction (XRD) analyses

Discover Applied Sciences

XRD analysis was conducted to examine the crystalline nature and structural characteristics of plant-mediated synthesized ZnO NPs. The XRD diffraction pattern revealed distinct peaks detected at 2θ angles of 31.64, 34.29, 36.12, 47.42, 56.49, 62.76, 66.32, 67.87, and 68.96 for ZnO NPs synthesized from C. dactylon. Similarly, 2θ values of 31.60, 34.24, 36.07, 47.39, 56.43, 62.72, 66.26, 67.80, and 68.94 for ZnO NPs synthesized from A. vulgaris and finally, 2θ values of 31.60, 34.25, 36.07, 47.37, 56.44, 62.71, 66.36, 67.82, and 68.97 for ZnO NPs synthesized from A. catechu associated to their miller indices of (100), (002), (101), (102), (110), (103), (200), (112) and (201) respectively as shown in Figure S5, S6, and S7, which is similar with those reported in previous literature [22, 26, 71].

The observed pattern corresponds to a hexagonal wurtzite structure of ZnO NPs, featuring lattice parameters a = 3.26 (Å) and c = 5.23 (Å) as evidenced by its conformity with JCPDS card no. 36–1451 as depicted in Fig. 3, a consistency observed in multiple studies [34, 35, 67]. The findings indicated all the identifiable peaks were specific to ZnO NPs and intense peaks signify no impurities detected in the preparation of ZnO NPs. The mean crystallite size was achieved by applying the Debye-Scherrer formula, yielding measurements of 18.97 nm, 16.98 nm, and 15.07 nm for ZnO NPs synthesized from C. dactylon, A. vulgaris, and A. catechu respectively as shown in Table S1, S2, and S3.

3.5 Scanning Electron Microscopy (SEM) analyses

SEM provides important information regarding surface morphology, aggregation, size, and distribution of nanoparticles [76]. Higher magnification shows a clearer image where NPs are seen to be identical in shape and dimension. SEM disclosed the uniform spherical structure of ZnO NPs, displaying slight agglomeration likely attributed to the Vander Waals clustering of smaller entities as shown in Fig. 4 below. Several works of the literature suggest that agglomeration is due to phytochemical moieties present on the particle surface, high surface area, polarity, and electrostatic attraction of biologically synthesized NPs, or it could be attributed to experimental parameters during the synthesis process such as variation in temperature and pH of the medium [71, 77, 78].

Various studies have documented the spherical shape of ZnO NPs at lower precursor concentrations and spherical mixed with hexagonal and cubical at higher concentrations [2, 79]. Similarly, using SEM images and the assistance of Image J software, the average size of ZnO NPs was calculated by assessing the mean length of the ten smallest particles observed in the image. The obtained mean diameter of ZnO NPs synthesized from C. dactylon, A. vulgaris, and A. catechu was 17.83 nm, 17.82 nm, and 18.5 nm, respectively. These values align well with the average size determined through XRD studies.

Fig. 3 XRD plot of ZnO NPs synthesized from three distinct plant extracts along with JCPDS Card of ZnO

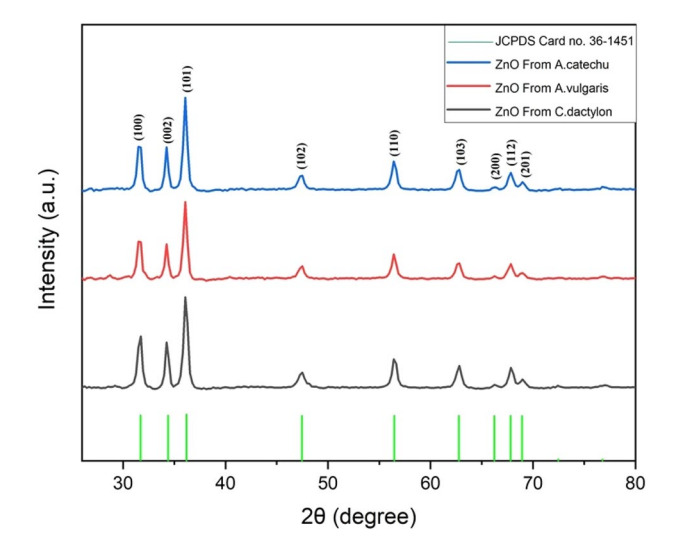
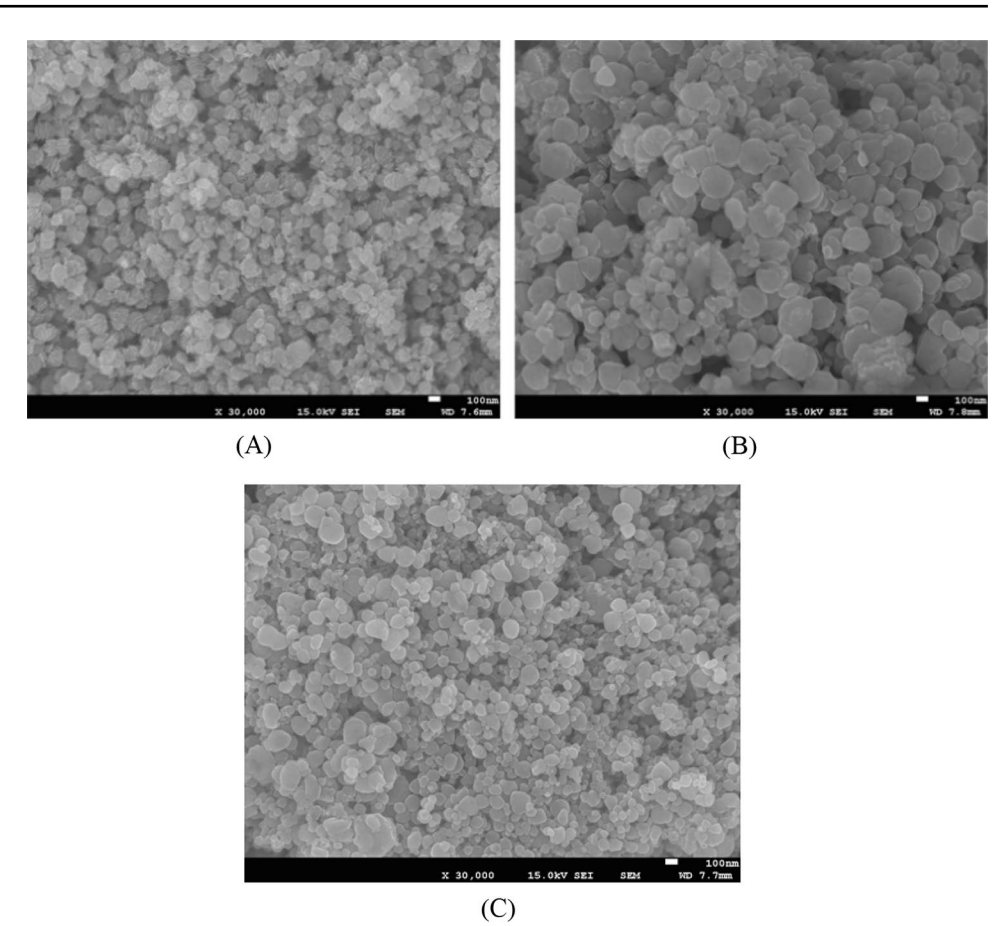




Fig. 4 SEM pictures of ZnO NPs obtained from **A** *C. dactylon*, **B** *A. vulgaris*, and **C** *A. catechu* respectively (scale bar at 100 nm)

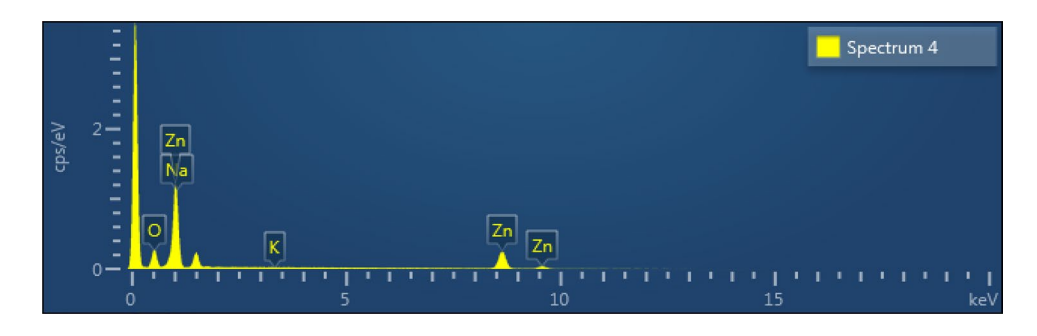


3.6 Energy dispersive X-ray spectroscopy (EDX) analyses

The elemental components, relative abundance, and presence of impurities in nanoparticles are demonstrated through EDX [76]. EDX revealed that the synthesized structure possesses the targeted elemental composition of zinc and oxygen along with traces of sodium and potassium. The existence of these additional elements can be ascribed to the occurrence of various metabolites present in the plant extract as illustrated in Figs. 5, S8, and S9. The detection of Zn and O peaks confirmed the existence of zinc in oxide form. In Figures, Zn and O signals were detected between (0–2) KeV, and two Zn signals were obtained between (8–10) KeV which is similar to those found in several literatures [2, 27, 80].

The weight % of Zn and O from *C. dactylon* was 74.44% and 20.08%, *A. vulgaris* was 69.76% and 21.75%, and *A. catechu* was 74.43% and 18.30% showing greater purity for ZnO NPs synthesized using *C. dactylon* and *A. catechu* as shown in Table S4-6 respectively. The wt. % peaks closely resemble those documented earlier in the biosynthesis of ZnO NPs [26, 78, 81]. The theoretical weight % of Zn in ZnO is 80.34% and the reduction of wt. % of Zn in the above compound is ascribed to the existence of a certain amount of sodium and potassium obtained from plant extract.

Fig. 5 EDX of ZnO NPs obtained from *C. dactylon*





Discover Applied Sciences

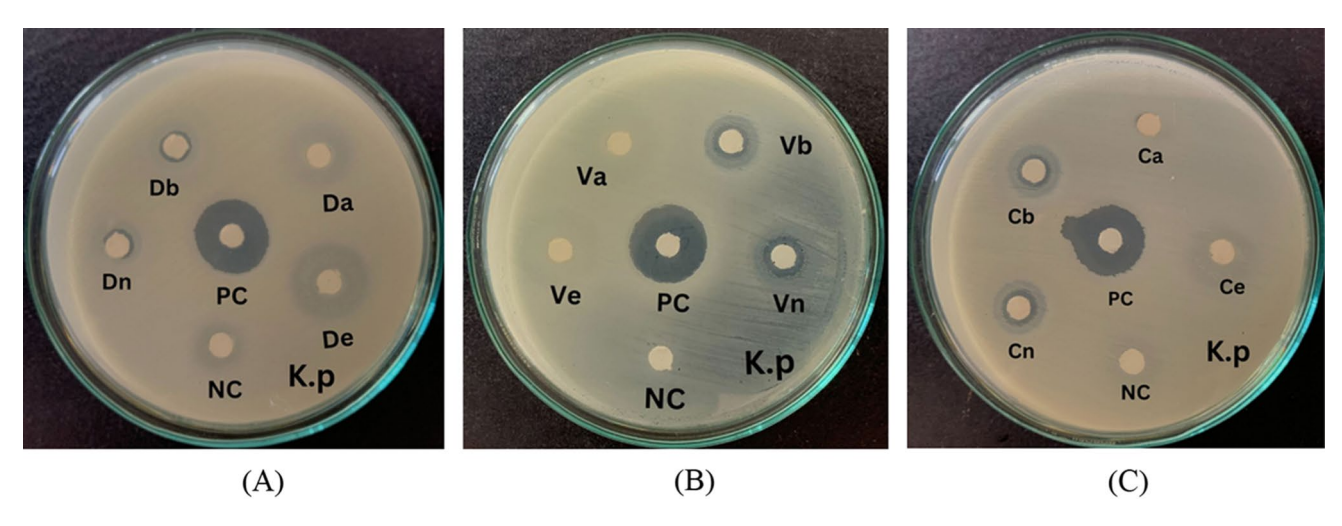


Fig. 6 Disc diffusion method of ZnO NPs, extract and blank of A C. dactylon, B A. vulgaris, and C A. catechu respectively against Klebsiella pneumoniae (KP)

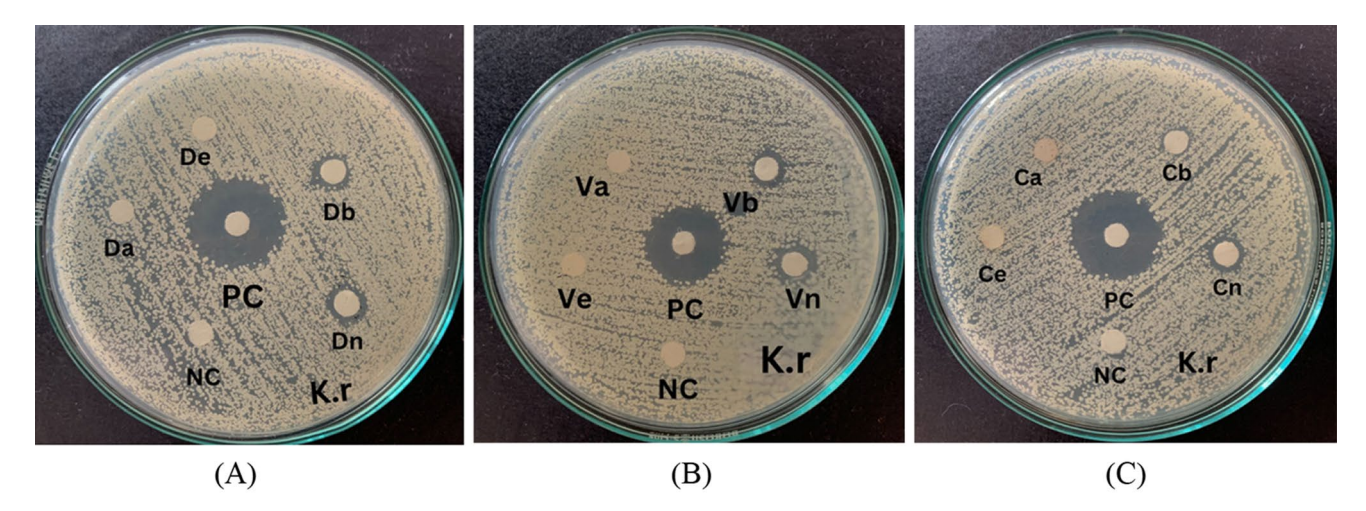


Fig. 7 Disc diffusion method of ZnO NPs, extract and blank of A C. dactylon, B A. vulgaris, and C A. catechu respectively against Kocuria rhizophila (KR)

3.7 Antibacterial susceptibility assay

The synthesized ZnO NPs were evaluated for their antibacterial efficacy against both gram-positive (Staphylococcus aureus, Kocuria rhizophila) and gram-negative bacteria (Klebsiella pneumonia, Shigella sonnei) by disc diffusion method [48]. Figures 6, S10, 7, and S11 below illustrate the zone of inhibition (ZOI) of ZnO NPs from different plant extracts, plant extracts only, and blanks of respective extracts (blank A contains plant extracts without Zn precursors following the synthesizing protocol whereas blank B contains Zn precursors without plant extracts following the synthesizing protocol). The findings showed the antibacterial effectiveness of ZnO NPs against both Gram-positive and Gram-negative bacteria.

Dn stands for ZnO NPs synthesized from C. dactylon, De stands for C. dactylon extract, Da stands for C. dactylon blank A, Db stands for blank B, PC signifies positive control (Neomycin) and NC signifies negative control (water). Similarly, Vn, Ve, Va, and Vb stand for ZnO NPs synthesized from A. vulgaris, A. vulgaris extract, and A. vulgaris blank A and blank B respectively. Likewise, Cn, Ce, Ca, and Cb stand for ZnO NPs synthesized from A. catechu, A. catechu extract, and A. catechu blank A and blank B respectively.

The NPs, plant extract, and blank all showed antibacterial activity against Klebsiella pneumonia. In comparison, ZnO NPs obtained from A. vulgaris and A. catechu (ZOI of 14 mm) showed better results than that of ZnO NPs from



C. dactylon (ZOI of 12 mm) which is equivalent to that obtained from previous literature of ZnO NPs synthesized from P. hysterophorous [82], (ZOI of 13.33 mm) and exceeds the ZOI of ZnO NPs synthesized from Albizia lebbeck [56], (ZOI of 7.30 mm). The antibacterial activity exhibited by blank A can be ascribed to the abundance of specific plant metabolites present, which have demonstrated potent antibacterial properties [43, 83], while blank B's antibacterial activity is probably due to the formation of ZnO through the experimental process as illustrated in Figure S4.

Similarly, The NPs and Blank B show antibacterial activity against *Shigella sonnei* (SS) However no activity was shown by given plant extracts and their blanks. In comparison, ZnO NPs obtained from *A. vulgaris* (ZOI of 9 mm) showed better results than both obtained from *A. catechu* and *C. dactylon* (ZOI of 8 mm).

In the same way, The ZnO NPs exhibited antibacterial efficacy against *Staphylococcus aureus* (SA). However, no activity was shown by plant extracts and respective blank. On comparing, ZnO NPs obtained from *A. catechu* (ZOI of 10 mm) showed slightly better antibacterial activity than that of both NPs obtained from *C. dactylon* and *A. vulgaris* (ZOI of 9 mm) which is equivalent to that obtained from previous literature of ZnO NPs synthesized from grape seed [40], *Cocos nucifera* [42], and *Euphorbia abyssinica* [41].

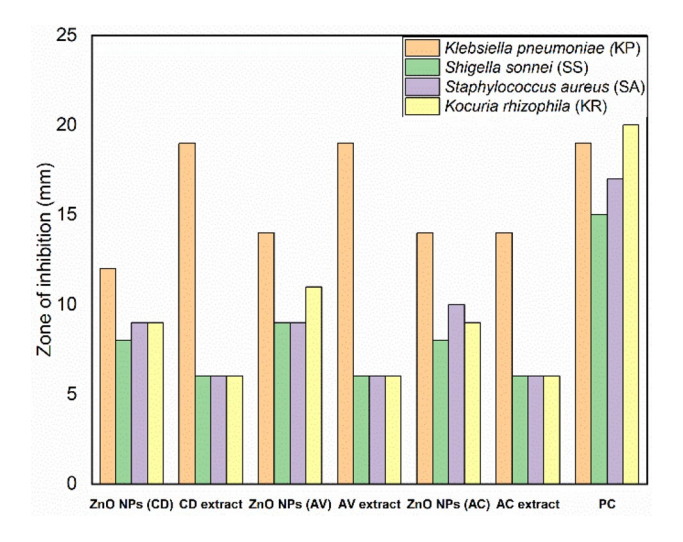
Likewise, The ZnO NPs from the different extracts and blank B show antibacterial activity against *Kocuria rhizophila* (KR). However, no activity of plant extracts and their respective blanks were observed. Upon comparison, ZnO NPs obtained from *A. vulgaris* (ZOI of 11 mm) showed slightly better activity than that of both ZnO NPs obtained from *C. dactylon* and *A. catechu* (ZOI of 9 mm) as shown in Table S7.

The results indicated variations in antibacterial efficacy among the different ZnO NPs. For instance, ZnO NPs from *A. vulgaris* and *A. catechu* exhibited better results against *Klebsiella pneumonia* compared to those synthesized from *C. dactylon*. Additionally, ZnO NPs synthesized from *A. vulgaris* showed superior activity against *Shigella sonnei*, while ZnO NPs synthesized from *A. catechu* demonstrated slightly better antibacterial effectiveness against *Staphylococcus aureus*. The findings suggest that the efficacy of ZnO NPs differed across various bacterial strains, indicating the choice of plant extract influences the antibacterial efficacy against specific pathogens.

These findings align well with the results documented in various sources [56, 84]. Similarly, The antibacterial potential of ZnO NPs produced with orange peel extract was evident against both *Escherichia coli* and *Staphylococcus aureus* [34]. Likewise, the *Artemisia pallens* extract-mediated ZnO NPs demonstrated inhibition zones measuring 12 mm, 7 mm, and 6 mm against *B. subtilis, S. aureus*, and *E. coli* respectively [35]. The inhibition zone for *Staphylococcus aureus* ranged from (8–12) nm when exposed to ZnO NPs concentrations synthesized using grape seed extract [40]. Similarly, A recent study on the antibacterial investigation was conducted on *S. aureus* (Gram-positive) and *E. coli* (Gram-negative) bacteria resulting in an effectiveness rate of 90% [78]. The ZnO NPs synthesized through *Euphorbia abyssinica* bark extract demonstrated ZOI measuring 11 nm, 10 nm, and 11 nm for *Staphylococcus aureus*, *Bacillus subtilis*, and *Escherichia coli* respectively [41]. Numerous investigations have confirmed that small biosynthesized ZnO NPs display antibacterial efficacy against both gram-positive and gram-negative strains due to increased surface area that can readily penetrate bacterial membranes and enhance antibacterial efficacy [85].

The chart shown in Fig. 8 reflects the antibacterial efficacy of ZnO nanoparticles derived from various extracts, as well as the antibacterial effectiveness of the extracts themselves. The result indicated that *C. dactylon* extract, *A. vulgaris*, and *A. catechu* extract showed good antibacterial activity against *Klebsiella pneumoniae*, likely due to the

Fig. 8 Comparative graphical representation of bacterial inhibition zones of Plantmediated ZnO NPs and plant extracts on different bacterial strains, where CD refers to C. dactylon, AV refers to A. vulgaris and AC refers to A. catechu





presence of potent bioactive components. Similarly, ZnO NPs obtained from A. vulgaris extract showed overall good potency against all bacterial strains.

3.8 Cytotoxicity and cell viability analyses

Discover Applied Sciences

The cell viability and cytotoxicity plots shown in Fig. 9 demonstrate that all groups of ZnO NPs concentrations were viable except the samples with the higher dose of the ZnO NPs i.e., AC-50, AV-50, and CD-50. The viability of this cell line was found to be dependent on both the dose and incubation time with the ZnO NPs. Extending the incubation time from 24 to 72 h resulted in a positive effect on cell growth particularly for the lower doses. Numerous prior studies have reported the dose-dependent cytotoxic effect of ZnO NPs [86–89]. In a study led by Maede Hasannasab, lower concentrations of ZnO-NPs promoted the adhesion and multiplication of fibroblast cells whereas higher doses reversed the trend when higher doses were applied [90]. Morphological features of the ZnO-NPs had a significant influence on cancer cells. The shape, size, and concentrations of ZnO NPs are crucial factors that determine their effectiveness in combating cancer [91, 92]. The involvement of reactive oxygen species (ROS) in cell replication, differentiation, and transcription could be used to explain the increased proliferation of fibroblasts observed at lower concentrations of ZnO NPs [93, 94]. The fluorescence images in Fig. 10 showed the accelerated growth in cells as doses of the ZnO NPs increase but it's not the same with the higher dose. This means that the cells can only contain a certain level of concentration of the ZnO NPs to be viable. It was also evident from the plots of biocompatibility tests that the viability of ZnO NPs from the C. dactylon group was comparatively higher than the others. The biocompatibility of the green synthesized ZnO NPs makes it more susceptible for biological and therapeutic purposes like antiviral, anti-inflammatory, antioxidant, and anti-diabetic activities due to its positive effect on cell proliferation [9].

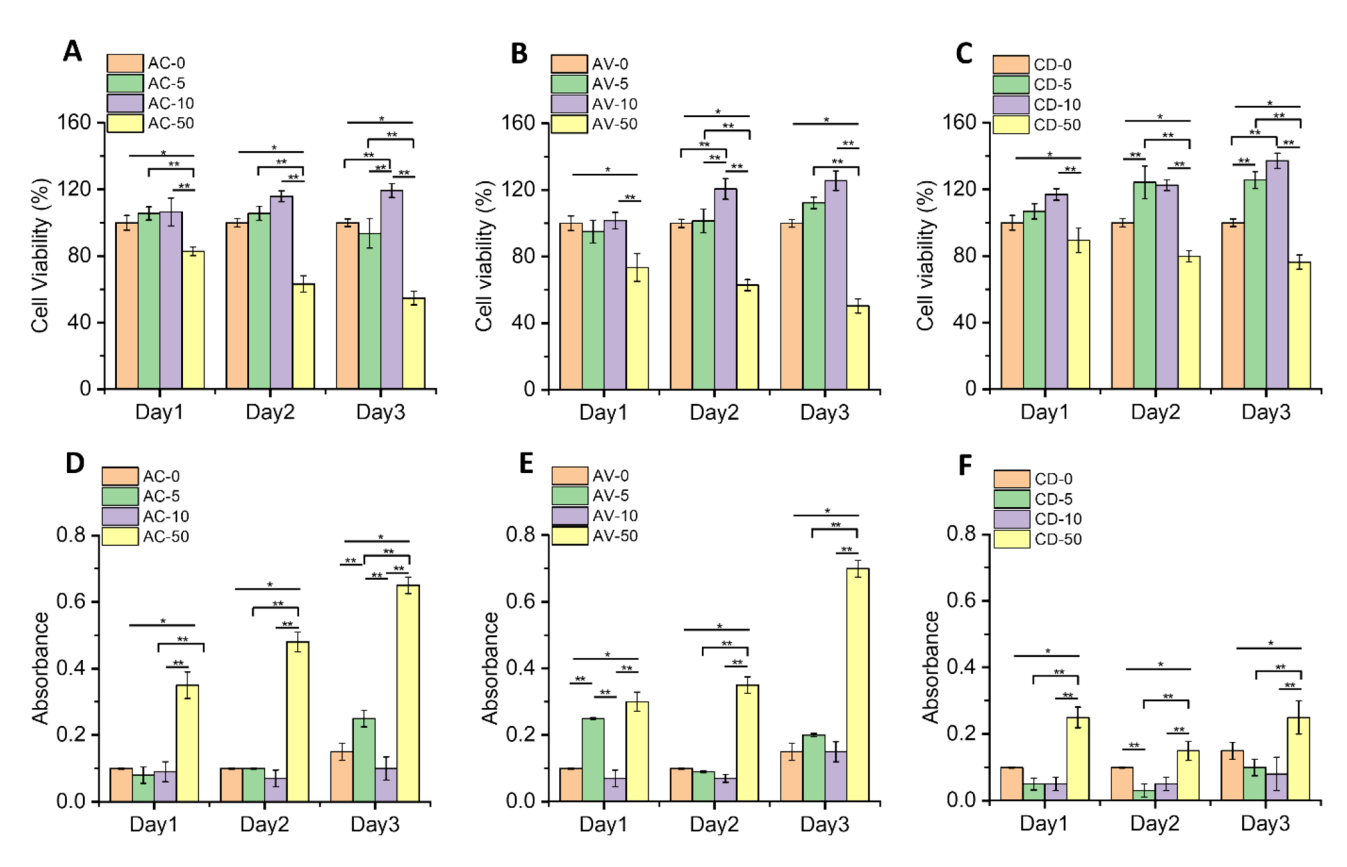


Fig. 9 In vitro performance of ZnO NPs and their impact on viability and toxicity of 3T3 fibroblast cells. A, B, and C represent the viability study (Alamar Blue assay) and D, E, and F represent the toxicity study (LDH absorbance assay) of the cultured cells with AC, AV, and CD samples, respectively. P-values less *p < 0.05 and **p < 0.01 were statistically significant



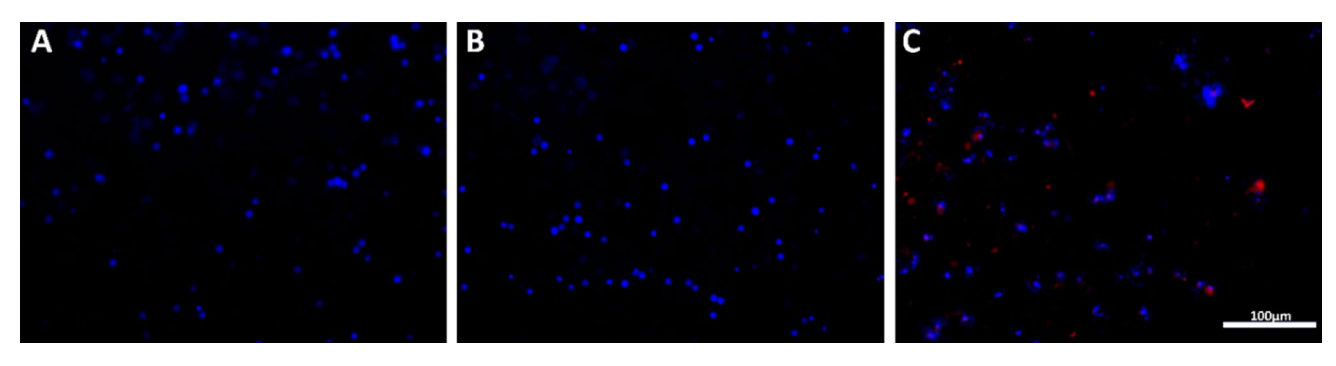


Fig. 10 Representative fluorescence microscopy images of NIH/3T3 fibroblast cells cultured with ZnO NPs. **A** (5 μ g/mL), **B** (10 μ g/mL), and **C** (50 μ g/mL) of ZnO NPs at day 3. The cytoskeleton was stained using rhodamine-phalloidin (red) and the nuclei were counterstained with DAPI (blue). (Scale bar = 100 μ m)

4 Conclusions

ZnO NPs can be synthesized utilizing the plant-mediated technique that is environmentally friendly and a good alternative to traditional techniques. The synthesized ZnO NPs were confirmed with UV-visible spectroscopy. The nature, size, and structure of ZnO NPs were revealed through XRD. FTIR Spectroscopy showed evidence of the incorporation of phytochemicals during ZnO NPs synthesis. SEM analysis demonstrated that ZnO NPs exhibited a spherical shape. Synthesized ZnO NPs exhibited antimicrobial effect and biocompatibility with NIH-3T3 mouse fibroblast cells. Among the ZnO nanoparticles (NPs) prepared from the three distinct extracts, those derived from *A. catechu* exhibited the smallest crystallite size. Furthermore, the percentage composition of Zn and O in the *A. catechu* NPs was superior to that of the other two extracts. In contrast, the SEM image of ZnO NPs obtained from *A. vulgaris* displayed a comparably spherical shape with slight agglomeration compared to the other two extracts. Moreover, both ZnO NPs synthesized from *A. catechu* and *A. vulgaris* demonstrated good antibacterial activity. Cell viability and toxicity analysis revealed that ZnO NPs prepared from *C. dactylon* exhibited relatively higher viability compared to the NPs obtained from the other extracts. Hence, the results of this study suggest that ZnO NPs synthesized ZnO NPs using *C. dactylon*, *A. vulgaris*, and *A. catechu* plant extract hold promising potential for biomedical applications.

Acknowledgements We are thankful to Agni Raj Koirala, the Korea Center for Artificial Photosynthesis, Sogang University for providing SEM and EDX data.

Author contributions Conceptualization: NP and NB; Synthesis and characterization: RA; Antibacterial assay: RA; Cytotoxicity assay: FT; Writing original draft: RA and FT; Editing: NP, AG. and NB. Review: KRS.; Funding acquisition: NB.

Funding Part of this work in NC A&T State University is supported by the National Science Foundation-Excellence in Research (NSF-EiR, 2100861).

Data availability The data used to support the findings of this study are included in the article.

Declarations

Ethics approval and consent to participate We have used locally available plant(s) or seeds in this study, which do not require permits/permissions/licenses from government authorities in Nepal.

Competing interests The authors declare that there is no conflict of interest regarding the publication of this paper.

Open Access This article is licensed under a Creative Commons Attribution 4.0 International License, which permits use, sharing, adaptation, distribution and reproduction in any medium or format, as long as you give appropriate credit to the original author(s) and the source, provide a link to the Creative Commons licence, and indicate if changes were made. The images or other third party material in this article are included in the article's Creative Commons licence, unless indicated otherwise in a credit line to the material. If material is not included in the article's Creative Commons licence and your intended use is not permitted by statutory regulation or exceeds the permitted use, you will need to obtain permission directly from the copyright holder. To view a copy of this licence, visit http://creativecommons.org/licenses/by/4.0/.



Discover Applied Sciences

References

- 1. Sati SC, Kour G, Bartwal AS, Sati MD. Biosynthesis of metal nanoparticles from leaves of *ficus palmata* and evaluation of their anti-inflammatory and anti-diabetic activities. Biochemistry. 2020;59:3019–25. https://doi.org/10.1021/acs.biochem.0c00388.
- 2. Maheo AR, Vithiya BSM, Arul Prasad TA, Mangesh VL, Perumal T, Al-Qahtani WH, Govindasamy M. Cytotoxic, antidiabetic, and antioxidant study of biogenically improvised *Elsholtzia blanda* and Chitosan-assisted zinc oxide nanoparticles. ACS Omega. 2023;8:10954–67. https://doi.org/10.1021/acsomega.2c07530.
- 3. Barth JV, Costantini G, Kern K. Engineering atomic and molecular nanostructures at surfaces. In nanoscience and technology. London: Macmillan Publishers Ltd; 2009. p. 67–75.
- 4. Zewde D, Geremew B. Biosynthesis of ZnO nanoparticles using *Hagenia abyssinica* leaf extracts; their photocatalytic and antibacterial activities. Environ Pollut Bioavail. 2022;34:224–35. https://doi.org/10.1080/26395940.2022.2081261.
- Hammad TM, Salem JK, Harrison RG. The Influence of Annealing Temperature on the Structure, Morphologies and Optical Properties of ZnO Nanoparticles. Superlattices and Microstructures. 2010;47:335–340. https://doi.org/10.1016/j.spmi.2009.11.007.
- 6. Halbus AF, Horozov TS, Paunov VN. Surface-modified zinc oxide nanoparticles for antialgal and antiyeast applications. ACS Appl Nano Mater. 2020;3:440–51. https://doi.org/10.1021/acsanm.9b02045.
- 7. Buzea C, Pacheco II, Robbie K. Nanomaterials and Nanoparticles: Sources and Toxicity. Biointerphases. 2007;2:MR17–71. https://doi.org/10.1116/1.2815690.
- 8. Sirelkhatim A, Mahmud S, Seeni A, Kaus NHM, Ann LC, Bakhori SKM, Hasan H, Mohamad D. Review on zinc oxide nanoparticles: antibacterial activity and toxicity mechanism. Nano-Micro Lett. 2015;7:219–42. https://doi.org/10.1007/s40820-015-0040-x.
- 9. Mandal AK, Katuwal S, Tettey F, Gupta A, Bhattarai S, Jaisi S, Bhandari DP, Shah AK, Bhattarai N, Parajuli N. Current research on zinc oxide nanoparticles: synthesis, characterization, and biomedical applications. Nanomaterials. 2022;12:3066. https://doi.org/10.3390/nano12173066.
- Maher S, Nisar S, Aslam SM, Saleem F, Behlil F, Imran M, Assiri MA, Nouroz A, Naheed N, Khan ZA, et al. Synthesis and characterization of ZnO nanoparticles derived from biomass (Sisymbrium Irio) and assessment of potential anticancer activity. ACS Omega. 2023. https://doi.org/10.1021/acsomega.2c07621.
- 11. Pandurangan M, Kim DH. In vitro toxicity of zinc oxide nanoparticles: a review. J Nanopart Res. 2015;17:158. https://doi.org/10.1007/s11051-015-2958-9.
- 12. Rani N, Rawat K, Saini M, Yadav S, Syeda S, Saini K, Shrivastava A. Comparative *in vitro* anticancer study of cisplatin drug with green synthesized ZnO nanoparticles on cervical squamous carcinoma (SiHa) cell lines. ACS Omega. 2023;8:14509–19. https://doi.org/10.1021/acsomega.2c08302.
- Ahmed S, Annu, Chaudhry SA, Ikram S. A Review on Biogenic Synthesis of ZnO Nanoparticles Using Plant Extracts and Microbes: A Prospect towards Green Chemistry. Journal of Photochemistry and Photobiology B: Biology. 2017;166:272–284. https://doi.org/10.1016/j.jphotobiol.2016.12.011.
- 14. Gharpure S, Yadwade R, Ankamwar B. Non-antimicrobial and non-anticancer properties of ZnO nanoparticles biosynthesized using different plant parts of *Bixa orellana*. ACS Omega. 2022;7:1914–33. https://doi.org/10.1021/acsomega.1c05324.
- 15. Yao BD, Chan YF, Wang N. Formation of ZnO Nanostructures by a Simple Way of Thermal Evaporation. Appl Phys Lett. 2002;81:757–9. https://doi.org/10.1063/1.1495878.
- 16. Rashid MI, Shahzad T, Shahid M, Ismail IMI, Shah GM, Almeelbi T. Zinc oxide nanoparticles affect carbon and nitrogen mineralization of phoenix dactylifera leaf litter in a sandy soil. J Hazard Mater. 2017;324:298–305. https://doi.org/10.1016/j.jhazmat.2016.10.063.
- 17. Dai ZR, Pan ZW, Wang ZL. Novel nanostructures of functional oxides synthesized by thermal evaporation. Adv Funct Mater. 2003;13:9–24. https://doi.org/10.1002/adfm.200390013.
- 18. Navas D, Fuentes S, Castro-Alvarez A, Chavez-Angel E. Review on sol-gel synthesis of perovskite and oxide nanomaterials. Gels. 2021;7:275. https://doi.org/10.3390/gels7040275.
- 19. Uhm YR, Han BS, Lee MK, Hong SJ, Rhee CK. Synthesis and characterization of nanoparticles of zno by levitational gas condensation. Mater Sci Eng A. 2007;449–451:813–6. https://doi.org/10.1016/j.msea.2006.02.427.
- Singh ThA, Sharma A, Tejwan N, Ghosh N, Das J, Sil PC. A state of the art review on the synthesis, antibacterial, antioxidant, antidiabetic and tissue regeneration activities of zinc oxide nanoparticles. Adv Coll Interface Sci. 2021;295: 102495. https://doi.org/10.1016/j.cis.2021. 102495.
- 21. Ismail AA, El-Midany A, Abdel-Aal EA, El-Shall H. Application of Statistical Design to Optimize the Preparation of ZnO Nanoparticles via Hydrothermal Technique. Materials Letters. 2005; 59:1924–1928. https://doi.org/10.1016/j.matlet.2005.02.027.
- 22. Sivasankarapillai VS, Krishnamoorthy N, Eldesoky GE, Wabaidur SM, Islam MA, Dhanusuraman R, Ponnusamy VK. One-pot green synthesis of ZnO nanoparticles using scoparia dulcis plant extract for antimicrobial and antioxidant activities. Appl Nanosci. 2022. https://doi.org/10.1007/s13204-022-02610-7.
- Shafique S, Jabeen N, Ahmad KS, Irum S, Anwaar S, Ahmad N, Alam S, Ilyas M, Khan TF, Hussain SZ. Green fabricated zinc oxide nanoformulated media enhanced callus induction and regeneration dynamics of *Panicum virgatum* L. PLoS ONE. 2020;15: e0230464. https://doi.org/10.1371/journal.pone.0230464.
- 24. Shah NI, Jabeen N, Irum S, Ahmad KS, Tauseef I, Khan TF, Anwaar S, Shafique S, Haleem SK, Mehmood A, et al. Environmentally benign and economical bio-fabrication of ZnO and Cr-doped ZnO nanoparticles using leaf extract of citrus reticulata for biological activities. Mater Today Commun. 2021;27: 102383. https://doi.org/10.1016/j.mtcomm.2021.102383.
- 25. Love AJ, Makarov VV, Sinitsyna OV, Shaw J, Yaminsky IV, Kalinina NO, Taliansky ME. A genetically modified tobacco mosaic virus that can produce gold nanoparticles from a metal salt precursor. Front Plant Sci. 2015. https://doi.org/10.3389/fpls.2015.00984.
- 26. Jayachandran A, Nair AS. Green synthesis and characterization of zinc oxide nanoparticles using cayratia pedata leaf extract. Biochem Biophys Rep. 2021;26:100995. https://doi.org/10.1016/j.bbrep.2021.100995.
- 27. Barzinjy AA, Azeez HH. Green synthesis and characterization of zinc oxide nanoparticles using *Eucalyptus globulus* labill. Leaf extract and zinc nitrate hexahydrate salt. SN Appl Sci. 2020;2:991. https://doi.org/10.1007/s42452-020-2813-1.



- (2024) 6:85
- 28. Gul H, Irum S, Ahmed W, Awais M, Khan MI. Iron oxide nanoparticle biosynthesis and potential application for hepatic cellular damages through antioxidant stress. Biomass Conv Bioref. 2023. https://doi.org/10.1007/s13399-023-04440-1.
- 29. Jeevanandam J, Chan YS, Danquah MK. Biosynthesis of metal and metal oxide nanoparticles. ChemBioEng Reviews. 2016;3:55–67. https://doi.org/10.1002/cben.201500018.
- 30. Gul H, Khan FS, Afzal U, Batool S, Saddick S, Awais M, Irum S, Malik MY, Ijaz Khan M, Alhazmi A, et al. Rumex hastatus derived silver nanoparticles development and their potential applications as hepatic-protection agent along with antimicrobial activity. J King Saud Univ Sci. 2021;33:101587. https://doi.org/10.1016/j.jksus.2021.101587.
- 31. Irum S, Jabeen N, Ahmad KS, Shafique S, Khan TF, Gul H, Anwaar S, Shah NI, Mehmood A, Hussain SZ. Biogenic iron oxide nanoparticles enhance callogenesis and regeneration pattern of recalcitrant *Cicer arietinum* L. PLoS ONE. 2020;15: e0242829. https://doi.org/10.1371/journal.pone.0242829.
- 32. Abdullah FH, Abu Bakar NHH, Abu Bakar M. Low temperature biosynthesis of crystalline zinc oxide nanoparticles from musa acuminata peel extract for visible-light degradation of methylene blue. Optik. 2020;206:164279. https://doi.org/10.1016/j.ijleo.2020.164279.
- 33. Bhattacharjee N, Som I, Saha R, Mondal S. A critical review on novel eco-friendly green approach to synthesize zinc oxide nanoparticles for photocatalytic degradation of water pollutants. Int J Environ Anal Chem. 2022. https://doi.org/10.1080/03067319.2021.2022130.
- 34. Thi TUD, Nguyen TT, Thi YD, Thi KHT, Phan BT, Pham KN. Green synthesis of ZnO nanoparticles using orange fruit peel extract for antibacterial activities. RSC Adv. 2020;10:23899–907. https://doi.org/10.1039/D0RA04926C.
- 35. Gomathi R, Suhana H. Green synthesis, characterization and antimicrobial activity of zinc oxide nanoparticles using *Artemisia pallens* plant extract. Inorg Nano-Metal Chem. 2020. https://doi.org/10.1080/24701556.2020.1852256.
- Chemingui H, Moulahi A, Missaoui T, Al-Marri AH, Hafiane A. A novel green preparation of zinc oxide nanoparticles with Hibiscus sabdariffa L.: photocatalytic performance evaluation of antioxidant and antibacterial activity. Environ Technol. 2022. https://doi.org/10.1080/09593 330.2022.2130108.
- 37. Ogunyemi SO, Abdallah Y, Zhang M, Fouad H, Hong X, Ibrahim E, Masum MMI, Hossain A, Mo J, Li B. Green synthesis of zinc oxide nanoparticles using different plant extracts and their antibacterial activity against *Xanthomonas oryzae* Pv. Oryzae. Artif Cells Nanomed Biotechnol. 2019;47:341–52. https://doi.org/10.1080/21691401.2018.1557671.
- 38. Hussain A, Oves M, Alajmi MF, Hussain I, Amir S, Ahmed J, Rehman MT, El-Seedi HR, Ali I. Biogenesis of ZnO nanoparticles using *Pandanus Odorifer* leaf extract: anticancer and antimicrobial activities. RSC Adv. 2019;9:15357–69. https://doi.org/10.1039/C9RA01659G.
- 39. Suresh D, Nethravathi PC, Rajanaika H, Nagabhushana H, Sharma SC. Green synthesis of multifunctional zinc oxide (ZnO) nanoparticles using *Cassia fistula* plant extract and their photodegradative, antioxidant and antibacterial activities. Mater Sci Semicond Process. 2015;31:446–54. https://doi.org/10.1016/j.mssp.2014.12.023.
- 40. Donmez S, Keyvan E. Green synthesis of zinc oxide nanoparticles using grape seed extract and evaluation of their antibacterial and antioxidant activities. Inorg Nano-Metal Chem. 2023. https://doi.org/10.1080/24701556.2023.2165687.
- 41. Faye G, Jebessa T, Wubalem T. Biosynthesis, characterisation and antimicrobial activity of zinc oxide and nickel doped zinc oxide nanoparticles using euphorbia abyssinica bark extract. IET Nanobiotechnol. 2022;16:25–32. https://doi.org/10.1049/nbt2.12072.
- 42. Rahman F, Majed Patwary MA, Bakar Siddique MA, Bashar MS, Haque MA, Akter B, Rashid R, Haque MA, Royhan Uddin AKM. Green synthesis of zinc oxide nanoparticles using cocos nucifera leaf extract: characterization, antimicrobial, antioxidant and photocatalytic activity. R Soc Open Sci. 2022;9:220858. https://doi.org/10.1098/rsos.220858.
- 43. Negi BS, Dave BP. In vitro antimicrobial activity of acacia catechu and its phytochemical analysis. Indian J Microbiol. 2010;50:369–74. https://doi.org/10.1007/s12088-011-0061-1.
- 44. Ekiert H, Pajor J, Klin P, Rzepiela A, Ślesak H, Szopa A. Significance of *Artemisia vulgaris* L. (Common Mugwort) in the history of medicine and its possible contemporary applications substantiated by phytochemical and pharmacological studies. Molecules. 2020;25:4415. https://doi.org/10.3390/molecules25194415.
- 45. Harlan JR, Wet JMJ. Sources of variation in *Cynodon dactylon* (L). Pers. 1. Crop Sci. 1969;9:774–8. https://doi.org/10.2135/cropsci1969. 0011183X000900060031x.
- 46. Mozafari AA, Vafaee Y, Shahyad M. Phytochemical Composition and in Vitro Antioxidant Potential of Cynodon Dactylon Leaf and Rhizome Extracts as Affected by Drying Methods and Temperatures. J Food Sci Technol. 2018;55:2220–2229. https://doi.org/10.1007/s13197-018-3139-5.
- 47. Holzwarth U, Gibson N. The Scherrer Equation versus the "Debye-Scherrer Equation." Nature Nanotech. 2011;6:534–534. https://doi.org/10.1038/nnano.2011.145.
- 48. Khadayat K, Sherpa DD, Malla KP, Shrestha S, Rana N, Marasini BP, Khanal S, Rayamajhee B, Bhattarai BR, Parajuli N. Molecular identification and antimicrobial potential of *streptomyces* species from nepalese soil. Int J Microbiol. 2020;2020:1–8. https://doi.org/10.1155/2020/8817467.
- 49. Raessi M, Alijani HQ, Nematollahi FF, Baty RS, El-Saber Batiha G, Khan AU, Hashemi N, Iravani S, Sharifi I, Aflatoonian M, et al. Barium carbonate nanostructures: biosynthesis and their biomedical applications. Ceram Int. 2021;47:21045–50. https://doi.org/10.1016/j.ceram int.2021.04.106.
- 50. Bastakoti BP, Bhattarai N, Ashie MD, Tettey F, Yusa S, Nakashima K. Single-micelle-templated synthesis of hollow barium carbonate nanoparticle for drug delivery. Polymers. 2023;15:1739. https://doi.org/10.3390/polym15071739.
- 51. Bhattarai SR, Saudi S, Khanal S, Aravamudhan S, Rorie JC, Bhattarai N. Electrodynamic assisted self-assembled fibrous hydrogel microcapsules: a novel 3D in vitro platform for assessment of nanoparticle toxicity. RSC Adv. 2021;11:4921–34. https://doi.org/10.1039/D0RA09189H.
- 52. Tatum SD, Saudi S, Tettey F, Bhandari RK, Bhattarai NA. Novel hydrogel-bronchial epithelial cell spheroids for toxicological evaluation. Biomed Sci Instrum. 2021. https://doi.org/10.34107/KSZV7781.10406.
- 53. Khanal S, Bhattarai SR, Sankar J, Bhandari RK, Macdonald JM, Bhattarai N. Nano-fibre integrated microcapsules: a nano-in-micro platform for 3D cell culture. Sci Rep. 2019;9:13951. https://doi.org/10.1038/s41598-019-50380-0.
- 54. Tettey F, Saudi S, Davies D, Shrestha S, Johnson K, Fialkova S, Subedi K, Bastakoti BP, Sankar J, Desai S, et al. Fabrication and characterization of Zn particle incorporated fibrous scaffolds for potential application in tissue healing and regeneration. ACS Appl Mater Interfaces. 2023. https://doi.org/10.1021/acsami.3c09793.



- 55. Tettey F, Siler-Dearring J, Moody A, Bhattarai N. Preparation and characterization of poliglecaprone-incorporated polycaprolactone composite fibrous scaffolds. Fibers. 2023;11:82.
- 56. Umar H, Kavaz D, Rizaner N. Biosynthesis of zinc oxide nanoparticles using albizia lebbeck stem bark, and evaluation of its antimicrobial, antioxidant, and cytotoxic activities on human breast cancer cell lines. Int J Nanomedicine. 2018;14:87–100. https://doi.org/10.2147/JJN. \$186888
- 57. Kumari M. Radha Kumar M. Zhang B. Amarowicz R. Puri S. Pundir A. Rathour S. Kumari N. Chandran D. et al. Acacia catechu (L.f.) Willd.: A Review on Bioactive Compounds and Their Health Promoting Functionalities. Plants. 2022;11:3091. https://doi.org/10.3390/plants1122
- 58. Adhikari B, Aryal B, Bhattarai B. A comprehensive review on the chemical composition and pharmacological activities of Acacia catechu (L.f.) Willd. J Chem. 2021. https://doi.org/10.1155/2021/2575598.
- 59. Kunwar RM, Shrestha KP, Bussmann RW. Traditional herbal medicine in far-West Nepal: a pharmacological appraisal. J Ethnobiol Ethnomed. 2010;6:35. https://doi.org/10.1186/1746-4269-6-35.
- 60. Patel JD, Kumar V, Bhatt SA. Antimicrobial screening and phytochemical analysis of the resin part of Acacia Catechu. Pharm Biol. 2009;47:34– 7. https://doi.org/10.1080/13880200802400527.
- 61. Wang J, Zhu F, Zhou XM, Niu CY, Lei CL. Repellent and fumigant activity of essential oil from artemisia vulgaris to Tribolium castaneum (Herbst) (Coleoptera: Tenebrionidae). J Stored Prod Res. 2006;42:339-47. https://doi.org/10.1016/j.jspr.2005.06.001.
- Bisht D, Kumar D, Kumar D, Dua K, Chellappan DK. Phytochemistry and pharmacological activity of the genus artemisia. Arch Pharm Res. 2021;44:439-74. https://doi.org/10.1007/s12272-021-01328-4.
- Savadi S, Vazifedoost M, Didar Z, Nematshahi MM, Jahed E. Phytochemical analysis and antimicrobial/antioxidant activity of Cynodon dactylon (L.) Pers. Rhizome methanolic extract. J Food Qual. 2020;2020: e5946541. https://doi.org/10.1155/2020/5946541.
- 64. Magalhães-Ghiotto GAV, Oliveira AMD, Natal JPS, Bergamasco R, Gomes RG. Green nanoparticles in water treatment: a review of research trends, applications, environmental aspects and large-scale production. Environ Nanotechnol Monit Manag. 2021;16: 100526. https:// doi.org/10.1016/j.enmm.2021.100526.
- 65. Jeevanandam J, Barhoum A, Chan YS, Dufresne A, Danquah MK. Review on nanoparticles and nanostructured materials: history, sources. Toxicity Regul Beilstein J Nanotechnol. 2018;9:1050-74. https://doi.org/10.3762/bjnano.9.98.
- Athanassiou CG, Kavallieratos NG, Benelli G, Losic D, Usha Rani P, Desneux N. Nanoparticles for Pest Control: Current Status and Future Perspectives. J Pest Sci. 2018;91:1-15. https://doi.org/10.1007/s10340-017-0898-0.
- 67. Al Sharie AH, El-Elimat T, Darweesh RS, Swedan S, Shubair Z, Al-Qiam R, Albargi H. Green synthesis of zinc oxide nanoflowers using Hypericum triquetrifolium extract: characterization, antibacterial activity and cytotoxicity against lung cancer A549 Cells. Appl Organomet Chem. 2020. https://doi.org/10.1002/aoc.5667.
- 68. Zak AK, Abrishami ME, Majid WHA, Yousefi R, Hosseini SM. Effects of annealing temperature on some structural and optical properties of ZnO nanoparticles prepared by a modified sol-gel combustion method. Ceramics Int. 2011;37:393–8. https://doi.org/10.1016/j.ceram int.2010.08.017.
- 69. Wang F-H, Chang C-L. Effect of substrate temperature on transparent conducting Al and F co-doped ZnO thin films prepared by rf magnetron sputtering. Appl Surf Sci. 2016;370:83-91. https://doi.org/10.1016/j.apsusc.2016.02.161.
- Gawade VV, Gavade NL, Shinde HM, Babar SB, Kadam AN, Garadkar KM. Green synthesis of ZnO nanoparticles by using calotropis procera leaves for the photodegradation of methyl orange. J Mater Sci: Mater Electron. 2017;28:14033-9. https://doi.org/10.1007/ s10854-017-7254-2.
- 71. Sajjad A, Bhatti SH, Ali Z, Jaffari GH, Khan NA, Rizvi ZF, Zia M. Photoinduced fabrication of zinc oxide nanoparticles: transformation of morphological and biological response on light irradiance. ACS Omega. 2021;6:11783–93. https://doi.org/10.1021/acsomega.1c01512.
- 72. Hariharan D, Srinivasan K, Nehru LC. Synthesis and characterization of Tio2 nanoparticles using cynodon dactylon leaf extract for antibacterial and anticancer (A549 Cell Lines) activity. J Nanomed Res. 2017;5(6):00138. https://doi.org/10.15406/jnmr.2017.05.00138.
- 73. Sharma RK, Tahiliani S, Jain N, Priyadarshi R, Chhangani S, Purohit SD, Joshi P. Cynodon dactylon leaf extract assisted green synthesis of silver nanoparticles and their anti-microbial activity. Adv Sci Eng Med. 2013;5:858-63. https://doi.org/10.1166/asem.2013.1352.
- 74. Depciuch J, Kasprzyk I, Roga E, Parlinska-Wojtan M. Analysis of morphological and molecular composition changes in allergenic artemisia vulgaris L. Pollen under traffic pollution using SEM and FTIR spectroscopy. Environ Sci Pollut Res. 2016;23:23203–14. https://doi.org/10. 1007/s11356-016-7554-8.
- 75. Samant L, Jose S, Rose NM, Shakyawar DB. Antimicrobial and UV protection properties of cotton fabric using enzymatic pretreatment and dyeing with Acacia Catechu. J Nat Fibers. 2022;19:2243-53. https://doi.org/10.1080/15440478.2020.1807443.
- 76. Dawadi S, Katuwal S, Gupta A, Lamichhane U, Thapa R, Jaisi S, Lamichhane G, Bhattarai DP, Parajuli N. Current research on silver nanoparticles: synthesis, characterization, and applications. J Nanomater. 2021;2021: e6687290. https://doi.org/10.1155/2021/6687290.
- 77. Bandeira M, Giovanela M, Roesch-Ely M, Devine DM, Da Silva Crespo J. Green synthesis of zinc oxide nanoparticles: a review of the synthesis methodology and mechanism of formation. Sustain Chem Pharm. 2020;15: 100223. https://doi.org/10.1016/j.scp.2020.100223.
- Chandrasekar LP, Sethuraman BD, Subramani M, Mohandos S. Green synthesised ZnO nanoparticles from plectranthus amboinicus plant extract: removal of safranin- o and malachite green dyes & anti-bacterial activity. Int J Environ Anal Chem. 2023. https://doi.org/10.1080/ 03067319.2023.2190458.
- 79. Kaningini AG, Azizi S, Sintwa N, Mokalane K, Mohale KC, Mudau FN, Maaza M. Effect of optimized precursor concentration, temperature, and doping on optical properties of ZnO nanoparticles synthesized via a green route using bush tea (Athrixia Phylicoides DC.) leaf extracts. ACS Omega. 2022;7:31658–66. https://doi.org/10.1021/acsomega.2c00530.
- 80. Chaudhuri SK, Malodia L. Biosynthesis of zinc oxide nanoparticles using leaf extract of calotropis gigantea: characterization and its evaluation on tree seedling growth in nursery stage. Appl Nanosci. 2017;7:501–12. https://doi.org/10.1007/s13204-017-0586-7.
- 81. Aida MS, Alonizan N, Zarrad B, Hjiri M. Influence of plant extract on the homogeneous and heterogeneous green chemistry synthesis of nanostructured ZnO. J Taibah Univ Sci. 2023;17:2179819. https://doi.org/10.1080/16583655.2023.2179819.
- Umavathi S, Mahboob S, Govindarajan M, Al-Ghanim KA, Ahmed Z, Virik P, Al-Mulhm N, Subash M, Gopinath K, Kavitha C. Green synthesis of ZnO nanoparticles for antimicrobial and vegetative growth applications: a novel approach for advancing efficient high quality health care to human wellbeing. Saudi J of Biol Sci. 2021;28:1808–15. https://doi.org/10.1016/j.sjbs.2020.12.025.



- 83. Haile AB, Jiru TM. Antibacterial effects of artemisia afra leaf crude extract against some selected multi-antibiotic resistant clinical pathogens. Ethiop J Health Sci. 2022;32:651–60. https://doi.org/10.4314/ejhs.v32i3.22.
- 84. Faisal S, Jan H, Shah SA, Shah S, Khan A, Akbar MT, Rizwan M, Jan F, Wajidullah; Akhtar, N., et al. Green synthesis of zinc oxide (ZnO) nanoparticles using aqueous fruit extracts of myristica fragrans: their characterizations and biological and environmental applications. ACS Omega. 2021;6:9709–22. https://doi.org/10.1021/acsomega.1c00310.
- 85. Hernández-Díaz JA, Garza-García JJ, Zamudio-Ojeda A, León-Morales JM, López-Velázquez JC, García-Morales S. Plant-mediated synthesis of nanoparticles and their antimicrobial activity against phytopathogens. J Sci Food Agric. 2021;101:1270–87. https://doi.org/10.1002/jsfa.10767.
- 86. Sana SS, Kumbhakar DV, Pasha A, Pawar SC, Grace AN, Singh RP, Nguyen V-H, Le QV, Peng W. Crotalaria verrucosa leaf extract mediated synthesis of zinc oxide nanoparticles: assessment of antimicrobial and anticancer activity. Molecules. 2020;25:4896. https://doi.org/10.3390/molecules25214896.
- 87. Gao Y, Arokia Vijaya Anand M, Ramachandran V, Karthikkumar V, Shalini V, Vijayalakshmi S, Ernest D. Biofabrication of zinc oxide nanoparticles from aspergillus niger, their antioxidant, antimicrobial and anticancer activity. J Clust Sci. 2019;30:937–46. https://doi.org/10.1007/s10876-019-01551-6.
- 88. Vidhya E, Vijayakumar S, Prathipkumar S, Praseetha PK. Green way biosynthesis: characterization, antimicrobial and anticancer activity of ZnO nanoparticles. Gene Rep. 2020;20: 100688. https://doi.org/10.1016/j.genrep.2020.100688.
- 89. Khara G, Padalia H, Moteriya P, Chanda S. Peltophorum pterocarpum flower-mediated synthesis, characterization, antimicrobial and cytotoxic activities of ZnO nanoparticles. Arab J Sci Eng. 2018;43:3393–401. https://doi.org/10.1007/s13369-017-2875-6.
- 90. Hasannasab M, Nourmohammadi J, Dehghan MM, Ghaee A. Immobilization of bromelain and ZnO nanoparticles on silk fibroin nanofibers as an antibacterial and anti-inflammatory burn dressing. Int J Pharm. 2021;610: 121227. https://doi.org/10.1016/j.ijpharm.2021.121227.
- 91. Motazedi R, Rahaiee S, Zare M. Efficient biogenesis of ZnO nanoparticles using extracellular extract of saccharomyces cerevisiae: evaluation of photocatalytic, cytotoxic and other biological activities. Bioorg Chem. 2020;101: 103998. https://doi.org/10.1016/j.bioorg.2020. 103998.
- 92. Dobrucka R, Długaszewska J. Biosynthesis and antibacterial activity of ZnO nanoparticles using trifolium pratense flower extract. Saudi J Biol Sci. 2016;23:517–23. https://doi.org/10.1016/j.sjbs.2015.05.016.
- 93. Goldkorn T, Balaban N, Matsukuma K, Chea V, Gould R, Last J, Chan C, Chavez C. EGF-receptor phosphorylation and signaling are targeted by H₂O₂ redox stress. Am J Respir Cell Mol Biol. 1998;19:786–98. https://doi.org/10.1165/ajrcmb.19.5.3249.
- 94. Augustine R, Malik HN, Singhal DK, Mukherjee A, Malakar D, Kalarikkal N, Thomas S. Electrospun polycaprolactone/ZnO nanocomposite membranes as biomaterials with antibacterial and cell adhesion properties. J Polym Res. 2014;21:347. https://doi.org/10.1007/s10965-013-0347-6.

Publisher's Note Springer Nature remains neutral with regard to jurisdictional claims in published maps and institutional affiliations.

